JOSEPHSON QUANTUM BITS BASED ON A COOPER PAIR BOX

Denis Vion

CEA-Saclay, Orme des merisiers,
91191 Gif sur Yvette Cedex , France

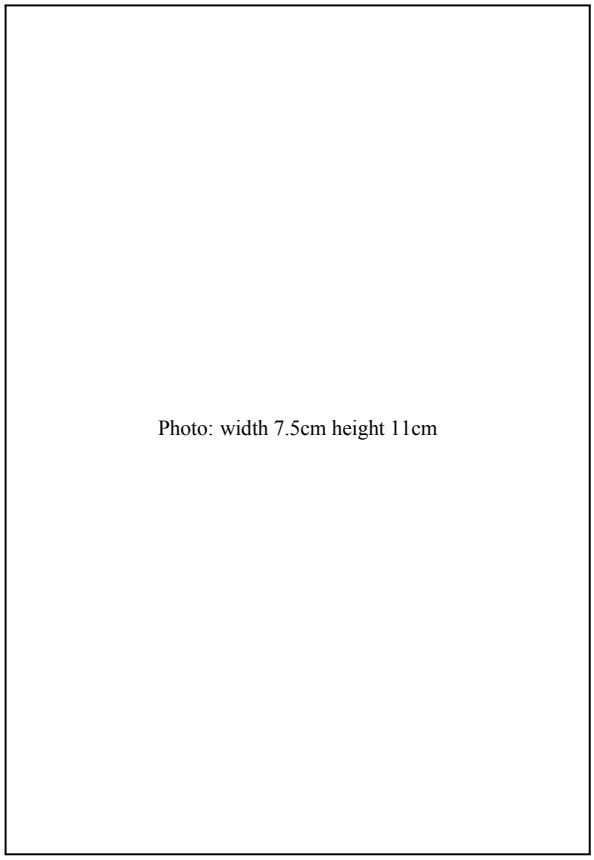
Photo: width 7.5cm height 11cm

Contents

1. Introduction

The present chapter is devoted to a particular type of electrical circuit that has been used to develop solid state quantum bit prototypes. These circuits being superconducting and involving tunneling of Cooper pairs between two superconducting electrodes, they belong to the family of Josephson qubits previously introduced in this book [1]. They are all based on the same simple device, the Cooper pair box (CPB), and are all driven by a gate electrode coupled to the charge of a small electrode. For that reason, they are often considered as forming the so-called "charge qubits" sub-family, although they essentially share the same physics with other Josephson qubits [2, 3]: their quantum state can be easily manipulated, whereas reading this state out with a high efficiency is a difficult task. Moreover, preserving their quantum coherence is a challenge (even at ultra low temperature) due to their "macroscopic" character.

This chapter is organized in six sections. After this introduction, the second section presents the Cooper pair box device in its basic version and in its improved version: the split CPB. The energy spectrum is derived as a function of the external parameters controlling the Hamiltonian and the physical properties of the corresponding eigenstates are pointed out. In the third section, we show how the two lowest energy eigenstates form a qubit, how this qubit can be manipulated with DC voltage pulses or resonant microwave pulses, and how it can be measured following various strategies. Three experiments that have demonstrated coherent control of the CPB state are also presented. Then, in section 4, we present a very simple approach to decoherence in CPBs. Considering a particular CPB device (the Quantronium) as an example, we list its different possible decoherence sources and we calculate the different physical quantities that characterize how coherence of its quantum state is lost. From these considerations, we infer design rules for Josephson qubits. Then, we present different experiments that have been used to measure the effective coherence time of a real device. Finally, we address in section 5 the problem of making a 2-qubit-gate with two capacitively coupled CPBs.

2. The Cooper pair box

2.1. The basic Cooper pair box circuit

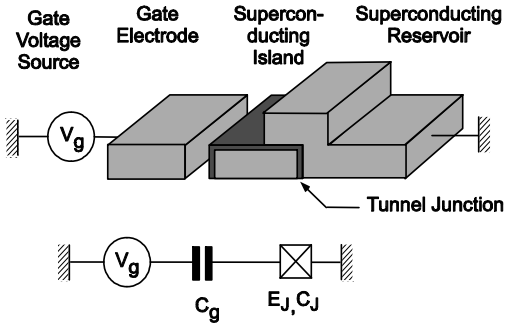

Fig. 1. *The basic Cooper pair box. Top: Schematic representation of the Cooper pair box showing the superconducting island and reservoir, the Josephson junction with energy E_J and capacitance C_J, the gate, and the voltage source V_g. Bottom: Corresponding electrical schematic drawing.*

The basic Cooper pair box (CPB) is the simplest device which combines Josephson [4] and Coulomb blockade effects [5]. It is a simplified version of a Josephson device proposed in 1987 [6], and consists [7] of a small BCS superconducting electrode, called the island, connected to a BCS superconducting reservoir by a Josephson junction with capacitance C_J and Josephson energy E_J. The island can be biased by a voltage source V_g in series with a gate capacitance C_g (see Fig. 1). In addition to E_J, the box has a second characteristic energy, the Coulomb energy E_C of a single Cooper Pair in excess in the island, with respect to electrical neutrality:

$$E_C = \frac{(2e)^2}{2C_\Sigma} \,, \tag{2.1}$$

where $C_\Sigma = C_g + C_J$ is the total capacitance of the island and e the electron charge. CPBs fabricated by conventional electron beam lithography having a capacitance C_Σ in the fF range (typical size of the junctions is 100nm $\times$ 100nm), E_C is typically of order of a few $k_B K$ (k_B is the Boltzmann constant). When the thermal energy $k_B T$ is reduced much below the BCS superconducting energy gap Δ of the electrodes, and when $E_C < 4\Delta$, all the electrons in the island and in the reservoirs are paired [8]. The Cooper pairs can tunnel through the Josephson junction and the only remaining degree of freedom of the system is the integer number $\mathbf{N}$ of Cooper pairs in excess or deficit on the island. Due to tunneling, $\mathbf{N}$

fluctuates quantum mechanically and has to be treated as an operator $\widehat{\mathbf{N}}$, whose eigenstates $|\mathbf{N}\rangle_c$ (index c stands for "pure charge") obey

$$\widehat{\mathbf{N}}\,|\mathbf{N}\rangle_c = \mathbf{N}\,|\mathbf{N}\rangle_c\,,\ \mathbf{N}\in\mathbb{Z}$$

and form a complete basis for the quantum states of the box. Introducing the operator $\widehat{\theta}$ conjugated to $\widehat{\mathbf{N}}$ by the dimensionless relationship $[\widehat{\theta},\widehat{\mathbf{N}}] = \mathbf{i}$, one defines the variable $\theta\in[0,2\pi[$, which is the phase of the Cooper pair condensate in the island. From the conjugation relationship, one deduces the effect of the operators $\exp(\mathbf{i}\widehat{\theta})$ and $\exp(-\mathbf{i}\widehat{\theta})$ on charge states:

$$\exp(\pm\mathbf{i}\widehat{\theta})\,|\mathbf{N}\rangle_c = |\mathbf{N}\pm 1\rangle_c\,. \tag{2.2}$$

The Hamiltonian of the CPB can now be expressed as a function of the $\widehat{\mathbf{N}}$ and/or $\widehat{\theta}$ operators.

2.2. Hamiltonian and energy spectrum

The Hamiltonian of the whole CPB circuit (including its voltage source) is written:

$$\widehat{H}(N_g) = \widehat{H}_{el} + \widehat{H}_J = E_C(\widehat{\mathbf{N}}-N_g)^2 - E_J\cos\widehat{\theta}\,, \tag{2.3}$$

where the first term corresponds to the electrostatic energy of the circuit, $N_g = C_gV_g/(2e)$ being the reduced gate charge, and where the second term accounts for the energy cost of a phase difference θ across the Josephson junction and is responsible for the tunneling of Cooper pairs. In order to find the eigenenergies and the corresponding eigenstates of the system, (2.3) is rewritten in a form involving only $\mathbf{N}$ or only θ. Using (2.2), one finds the Hamiltonian in the charge representation,

$$\widehat{H} = \sum_{\mathbf{N}\in\mathbb{Z}}\left[E_C(\mathbf{N}-N_g)^2\,|\mathbf{N}\rangle_c\,\langle\mathbf{N}|_c - \frac{E_J}{2}(|\mathbf{N}\rangle_c\,\langle\mathbf{N}+\mathbf{1}|_c + |\mathbf{N}+\mathbf{1}\rangle_c\,\langle\mathbf{N}|_c)\right]. \tag{2.4}$$

The energy spectrum associated to this Hamiltonian is discrete and periodic in N_g with period 1. We call $|k\rangle$ the energy eigenstates and E_k their associated energies sorted in increasing order, starting from $k=0$ for the ground state:

$$\widehat{H}\,|k\rangle = E_k\,|k\rangle\,,\ k\in\mathbb{N}. \tag{2.5}$$

For a given N_g, the lowest energy eigenstates can be found in the charge representation by truncating the pure charge state basis and by diagonalizing a finite version of the matrix that corresponds to (2.4).

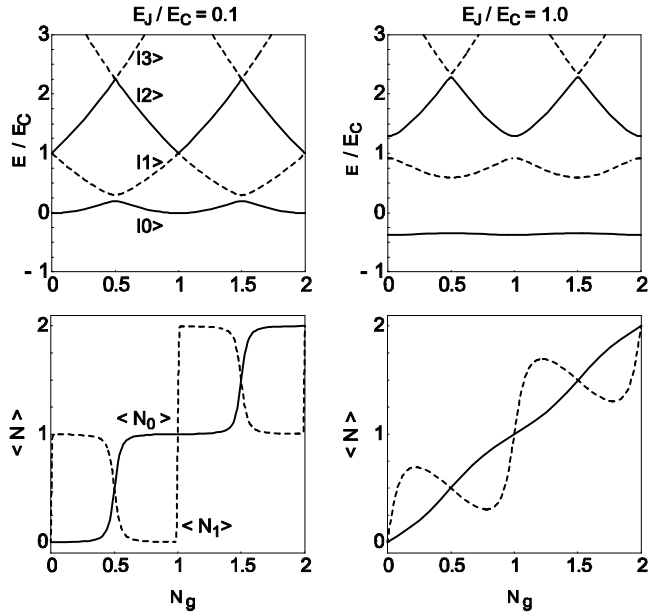

Fig. 2. Top: Energy levels of a Cooper pair box, normalized by the Cooper pair Coulomb energy E_C, as a function of the gate charge bias N_g, and for E_J/E_C ratios equal to 0.1 (left) and 1 (right). Bottom: Corresponding expectation values of the dimensionless box charges $\langle N \rangle$, for the energy eigenstates $|0\rangle$ (solid lines) and $|1\rangle$ (dotted lines).

Using $\widehat{\mathbf{N}} = (\mathbf{1}/\mathbf{i})\partial/\partial\theta$ in (2.3), one instead obtains the Hamiltonian in the phase representation and the Schrödinger equation for the $\Psi_k(\theta) = \langle\theta\,|k\rangle$ wavefunctions:

$$E_C(\frac{1}{\mathbf{i}}\frac{\partial}{\partial\theta} - N_g)^2\Psi_k(\theta) - E_J\cos(\theta)\Psi_k(\theta) = E_k\Psi_k(\theta)\ . \tag{2.6}$$

Both representations can of course be used equivalently to find the energy spectrum, which depends on N_g and on the E_J/E_C ratio, as shown on Fig. 2. When $E_J/E_C \ll 1$, the energy levels are very close to the electrostatic energies, except in the vicinity of the so-called charge degeneracy points defined by $N_g = 1/2\,(\mathrm{mod}\,1)$, where the degeneracy between the two lowest energy charge states is lifted up by an amount E_J. With increasing E_J/E_C, the modulation by N_g of the lowest eigenenergies becomes weaker and weaker.

It is interesting to note that except for precise combinations of E_J/E_C and N_g values, the energy spectrum of a CPB is highly anharmonic. Consequently, manipulating $|0\rangle$ and $|1\rangle$ without exciting higher energy states is possible. These two states are thus regarded as defining a qubit. We now compute explicitly the $|0\rangle$ and $|1\rangle$ states in order to evaluate their physical properties, which will be used to measure the quantum bit state.

2.3. Eigenstates in the charge and phase representations

Over an N_g period like the interval $[0, 1]$ and for $E_J/E_C < 2$, the energy eigenstates $|k\rangle = \sum_{\mathbf{N}\in\mathbb{Z}} a_{kN}\,|\mathbf{N}\rangle_c$ can be found with a high accuracy by simply diagonalizing a matrix (2.4) truncated to only seven charge states. The corresponding $\Psi_k(\theta)$ functions can be found by Fourier transform of the $|k\rangle$'s expressed in the charge representation or by solving directly the Schrödinger equation (2.6). This equation is close to a Mathieu equation and its solutions are [9]

$$\left\{\begin{array}{l} E_k = E_C\mathcal{M}_A(k+1-(k+1)[\mathrm{mod}\ 2] + 2n_g(-1)^k, q)/4 \\ \Psi_k(\theta) = \frac{\exp(\mathbf{i}N_g\theta)}{\sqrt{2\pi}}[\mathcal{M}_C(a,q,\frac{\theta}{2}) + \mathbf{i}(-1)^{k+1}\mathcal{M}_S(a,q,\frac{\theta}{2})] \end{array}\right. , \tag{2.7}$$

where $a = 4E_k/E_C$, $q = -2E_J/E_C$, $\mathcal{M}_C$ and $\mathcal{M}_S$ are the even and odd Mathieu functions, and $\mathcal{M}_A$ is the function giving the characteristic values of $\mathcal{M}_C$. Figure 3 shows the two lowest stationary states $|0\rangle$ and $|1\rangle$ both in the charge and phase representations, for $N_g = 0$ and $N_g = 1/2$, and for two different E_J/E_C ratios. For $E_J/E_C \ll 1$, the situation is rather simple since $|0\rangle$ and $|1\rangle$ are very close to the pure charge states $|\mathbf{0}\rangle_c$ or $|\mathbf{1}\rangle_c$ at $N_g \simeq 0$, and correspond to the symmetric and antisymmetric superpositions of these charge states at $N_g = 1/2$.

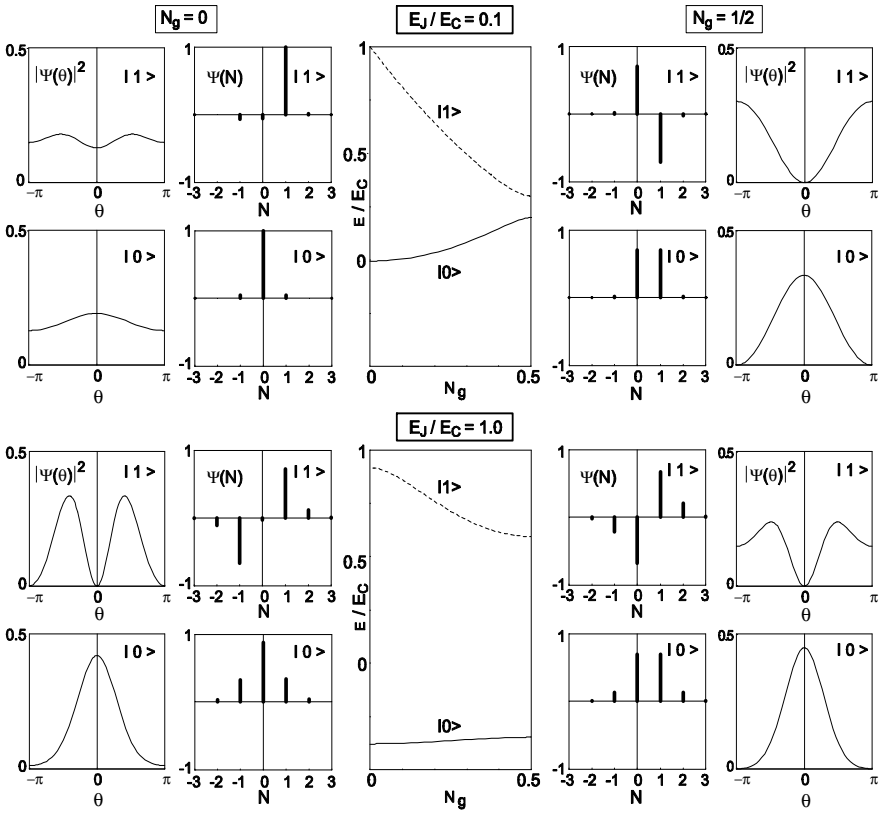

Fig. 3. Eigenenergies (middle panels) and wavefunctions of the $|0\rangle$ and $|1\rangle$ states in the charge and phase representations, for $N_g = 0$ (left panels) and for $N_g = 1/2$ (right panels), and for E_J/E_C ratios equal to 0.1 (top panels) and 1 (bottom panels). The $\Psi_k(N)$ eigenvectors are directly represented since they can be chosen real, whereas the $\Psi_k(\theta)$ wavefunctions are represented by their modulus squared.

In this limit, it is useful to restrict the basis to $(|\mathbf{0}\rangle_c, |\mathbf{1}\rangle_c)$, so that the Hamiltonian looks like that for a spin 1/2 (like any other two-level-system [10]), after dropping out a constant term that depends on N_g only:

$$\widehat{H} = -\frac{1}{2}\vec{\sigma}.\vec{H} \,, \tag{2.8}$$

where $\vec{\sigma} = \hat{\sigma}_x\vec{x} + \hat{\sigma}_y\vec{y} + \hat{\sigma}_z\vec{z}$ is the vector of Pauli matrices and $\vec{H} = E_J\vec{x} + E_C(1-2N_g)\vec{z}$. Introducing the angle $\alpha = \arctan\left[E_J/\left\{E_C(1-2N_g)\right\}\right]$, the eigenenergies and the eigenstates are in this case $\mp E_J\sqrt{1+\cot^2\alpha}$ and

$$\left[\begin{array}{l} |0\rangle = \cos(\alpha/2)\,|\mathbf{0}\rangle_c + \sin(\alpha/2)\,|\mathbf{1}\rangle_c \\ |1\rangle = -\sin(\alpha/2)\,|\mathbf{0}\rangle_c + \cos(\alpha/2)\,|\mathbf{1}\rangle_c \end{array}\right. , \tag{2.9}$$

respectively. For $E_J/E_C \sim 1$, the $|0\rangle$ and $|1\rangle$ states are, for any N_g, made up of coherent superpositions with significant contributions from at least three or four pure charge states (see Fig. 3), so that neither θ nor $\mathbf{N}$ are "good quantum numbers".

2.4. Expectation value of the box charge

The expectation value of the charge on the island or its dimensionless equivalent $\langle N_k\rangle = \langle k|\,\widehat{\mathbf{N}}\,|k\rangle$ is an interesting quantity which can be used to discriminate $|0\rangle$ from $|1\rangle$, and thus to read out a CPB-based-qubit. It depends linearly on the derivative of the energy levels with respect to N_g:

$$\frac{\partial\hat{H}}{\partial N_g} = 2E_C(N_g - \widehat{\mathbf{N}}) \Longrightarrow \langle N_k\rangle = N_g - \frac{1}{2E_C}\frac{\partial E_k}{\partial N_g} \,. \tag{2.10}$$

It is plotted in Fig. 2 for the two regimes already considered. For $E_J/E_C \ll 1$ and close to half integer values of N_g, $\langle N_0\rangle$ and $\langle N_1\rangle$ vary as opposite rounded staircases. Within the two charge states approximation, one deduces from (2.9) the shape of the steps for $N_g \in [0,1]$: $\langle N_0\rangle = \sin^2\alpha/2$ and $\langle N_1\rangle = \cos^2\alpha/2$. When E_J/E_C is increased, the steps are more and more rounded and have to be calculated numerically. It is important to note that the difference $\Delta N_{10} = \langle N_1\rangle - \langle N_0\rangle$ vanishes at the charge degeneracy points.

2.5. The split Cooper pair box

The split Cooper pair box is an improved CPB with a tunable Josephson energy and a second access port. It is obtained by splitting its Josephson junction into two junctions with respective Josephson energies $E_J(1+d)/2$ and $E_J(1-d)/2$, where $d \in [0,1]$ is an asymmetry coefficient (see Fig. 4). These two junctions

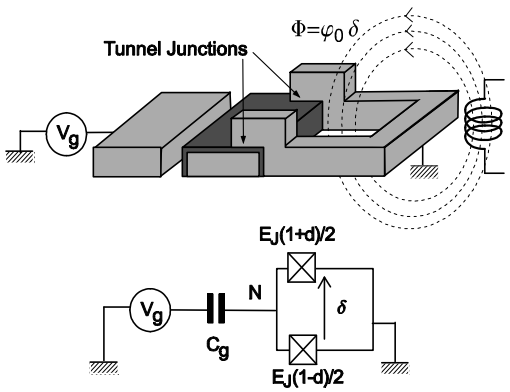

Fig. 4. *The split Cooper pair box. Top: Schematic representation showing the island, the two Josephson junctions connected to form a grounded superconducting loop, the gate circuit, and the magnetic flux bias. Bottom: Corresponding electrical drawing.*

are connected together to form a superconducting loop which can be biased by a magnetic flux Φ. Notice that the split CPB is similar to another Josephson device, the Bloch transistor [11] (also called the single Cooper pair transistor) that was first described in 1985. The split box has two degrees of freedom, which can be chosen either as the phase differences $\widehat{\delta_1}$ and $\widehat{\delta_2}$ across each junction, or as the linear forms $\widehat{\theta} = (\widehat{\delta_1} - \widehat{\delta_2})/2$ and $\widehat{\delta} = \widehat{\delta_1} + \widehat{\delta_2}$, which represent the phase of the island introduced previously and the phase difference across the series combination of the two junctions, respectively. The conjugate variable of $\widehat{\delta}$ is the integer number K of Cooper pairs which tunneled through both junctions.

The electrostatic "Hamiltonian" of the split CPB is that of a basic box [see (2.3)] with C_J representing now the sum of the two junction capacitances. Its Josephson "Hamiltonian" is the sum of the Josephson terms of the two junctions:

$$\widehat{H}_J^* = -E_J \frac{1+d}{2} \cos(\widehat{\delta_1}) - E_J \frac{1-d}{2} \cos(\widehat{\delta_2}) \tag{2.11}$$

$$= -E_J \cos(\frac{\widehat{\delta}}{2}) \cos(\widehat{\theta}) + dE_J \sin(\frac{\widehat{\delta}}{2}) \sin(\widehat{\theta}) \, . \tag{2.12}$$

The superconducting loop of a split CPB is designed such that its self inductance L is very small compared to the junction inductance $L_J = \varphi_0^2/E_J$, with $\varphi_0 = \hbar/2e$. Consequently, the magnetic potential energy term $\left(\varphi_0 \hat{\delta} - \Phi\right)^2 /2L$ attached to this inductance strongly fixes δ, which can be considered as a classical parameter $\delta = \Phi/\varphi_0$ imposed by the magnetic flux. Finally, the Hamiltonian

of the split box is

$$\widehat{H}(N_g,\delta) = E_C(\widehat{\mathbf{N}} - N_g)^2 - E_J^*(d,\delta)\cos[\widehat{\theta} + \Upsilon(d,\delta)]\ , \tag{2.13}$$

with [12]:

$$\begin{array}{l} E_J^*(d,\delta) = E_J\sqrt{\frac{1+d^2+(1-d^2)\cos(\delta)}{2}} \\ \tan\Upsilon(d,\delta) = -d\tan(\frac{\delta}{2})\ . \end{array} \tag{2.14}$$

A symmetric or almost symmetric ($d \approx 0$) split CPB is thus equivalent to a basic CPB but with a magnetostatically tunable [7] Josephson energy $E_J^* = E_J\cos(\delta/2)$. Its energy spectrum (see Fig. 5) is periodic in N_g (period 1) and 2π-periodic in δ, and can now be tuned by both the electric field applied to the gate electrode and by the magnetic flux threading the superconducting loop. For that reason, the split CPB has often been presented as a kind of artificial atom showing strong Stark and Zeeman effects.

Splitting the box has also a second interest: it opens a second access port to the device, which can be used to read out its quantum state [13–15]. The quantity to be measured on this port is the persistent current in the superconducting loop, its phase equivalent across the loop inductance, or the magnetic flux it produces. This persistent current is calculated below.

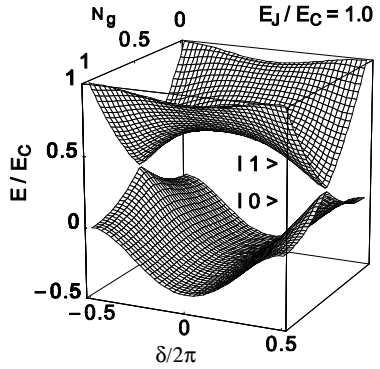

Fig. 5. Two lowest energy levels of a split Cooper pair box with $E_J/E_C = 1$, as a function of the two external parameters N_g and δ. The energy is normalized by the Cooper pair Coulomb energy E_C. The asymmetry coefficient $d = 2\%$ chosen here lifts up an energy degeneracy at ($N_g = 1/2, \delta = \pm\pi$).

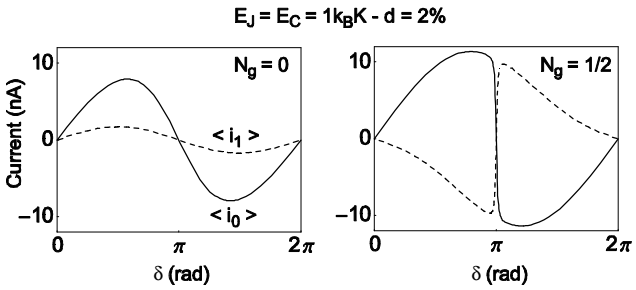

Fig. 6. Expectation value of the persistent loop currents $\langle i_0 \rangle$ for the ground state (solid line), and $\langle i_1 \rangle$ for the first excited state (dotted line), calculated for $E_C = E_J = 1$ k$_B$K, $d = 2\%$, $N_g = 0$ (left panel) and $N_g = 1/2$ (right panel).

2.6. Expectation value of the persistent current in the split box

The $\widehat{\delta}$ and $\widehat{K}$ operators being conjugate to each other, the operator associated to the current circulating in the loop of the split CPB is

$$\widehat{I} = (-2e)\,\frac{d\widehat{K}}{dt} = (-2e)\left(-\frac{1}{\hbar}\frac{\partial \widehat{H}}{\partial \delta}\right) . \tag{2.15}$$

The average loop current $\langle i_k \rangle$ of state $|k\rangle$ follows thus the generalized Josephson relation

$$\langle i_k(N_g, \delta)\rangle = \left\langle k \left| \widehat{I} \right| k \right\rangle = \frac{1}{\varphi_0}\frac{\partial E_k(N_g, \delta)}{\partial \delta} . \tag{2.16}$$

Like the energy spectrum, $\langle i_k \rangle$ currents are also 2π-periodic in δ and 1-periodic in N_g, the extrema of $\langle i_0 \rangle$ and $\langle i_1 \rangle$ being of the order of E_J/φ_0. Also, for N_g close to $1/2$ and $E_J < 3E_c$, $\langle i_0 \rangle$ and $\langle i_1 \rangle$ have opposite signs, as shown in Fig. 6. Note that the difference $\Delta i_{10} = \langle i_1 \rangle - \langle i_0 \rangle$ vanishes at $\delta = 0$ for all N_g.

Given the physical properties of the $|0\rangle$ and $|1\rangle$ CPB's states, we can now consider the different strategies for implementing, for driving and for reading a qubit based on these states.

3. The Cooper pair box as a quantum bit

As previously mentioned, the two orthogonal states chosen to define a CPB-based-qubit are its two lowest energy eigenstates $|0\rangle$ and $|1\rangle$. By varying N_g, the quantum state of the box can be manipulated within this subspace, provided that

the temperature is sufficiently low, that the N_g excursion is limited, and that the anharmonicity of the energy spectrum is large enough. To implement a qubit, the CPB has also to be coupled to a readout device able to discriminate its two states at a certain measuring point (N_{gm}, δ_m) in the space of the external parameters controlling its Hamiltonian. We consider here the case of a coupling between the box and its readout, weak enough so that it does not modify significantly the $|0\rangle$ and $|1\rangle$ states of the uncoupled box. When all these conditions are fulfilled, the CPB can be regarded as a fictitious dimensionless spin 1/2, $\vec{\sigma}$, with a Hamiltonian

$$\widehat{H}\left(N_g, \delta\right) = -\frac{1}{2}\vec{\sigma}.\vec{H}\left(N_g, \delta\right) \ . \tag{3.1}$$

This Hamiltonian can be expressed in any frame $R\{\vec{x}, \vec{y}, \vec{z}\}$ defined by

$$\left[\begin{array}{c} \vec{H}\left(N_{g0}, \delta_0\right) = h\nu_{01}\left(N_{g0}, \delta_0\right)\vec{z}\left(N_{g0}, \delta_0\right) \\ \partial\vec{H}/\partial N_g.\vec{y} = 0 \end{array}\right. , \tag{3.2}$$

where $\nu_{01}\left(N_g, \delta\right)$ is the transition frequency between $|0\rangle$ and $|1\rangle$ and (N_{g0}, δ_0) is a particular point in the parameter space. Note that the frame introduced with (2.8) when $E_J/E_C \ll 1$ is a limit case, for which the reference states $|\mathbf{0}\rangle_c$ and $|\mathbf{1}\rangle_c$ are almost equal to $|0\rangle$ and $|1\rangle$ for N_{g0} far away from the charge degeneracy point. The time variation of the spin state can be visualized in the so-called Bloch sphere picture, where the general quantum state

$$\cos(\theta_u/2)\exp(-\mathbf{i}\varphi_u/2)\,|0\rangle + \sin(\theta_u/2)\exp(\mathbf{i}\varphi_u/2)\,|1\rangle \ , \tag{3.3}$$

is represented by a vector with polar coordinates θ_u and φ_u, precessing around $\vec{H}$ with a frequency $|\vec{H}|/h$. We now consider the different ways of modifying $\vec{H}$ in order to manipulate $\vec{\sigma}$.

3.1. Manipulation of the Cooper pair Box quantum state

3.1.1. Constant perturbation applied suddenly to the Hamiltonian

The first method that was used experimentally in 1999 [16] to prepare a CPB-based-qubit in a coherent quantum superposition of its 2 states consists in applying to its gate (or to a second gate specially designed for that purpose) a trapezoidal N_g pulse with rise and fall times much shorter than $1/\nu_{01}$. This method was implemented on CPBs with $E_J/E_C \ll 1$, the gate charge being initially tuned at a value N_g of the order of 0.3 during a time long enough so that the qubit has relaxed to its ground state $|0\rangle \simeq |\mathbf{0}\rangle_c$. On the Bloch sphere drawn in the pure charge state referential (see left panel of Fig. 7), the initial situation corresponds to the spin parallel to the vector $\vec{H} = E_J\vec{x} + E_C(1-2N_g)\vec{z}$, the latter making a small angle $\alpha_0 \sim E_J/E_C(1-2N_g) \ll 1$ with $\vec{z}$. Then N_g is brought

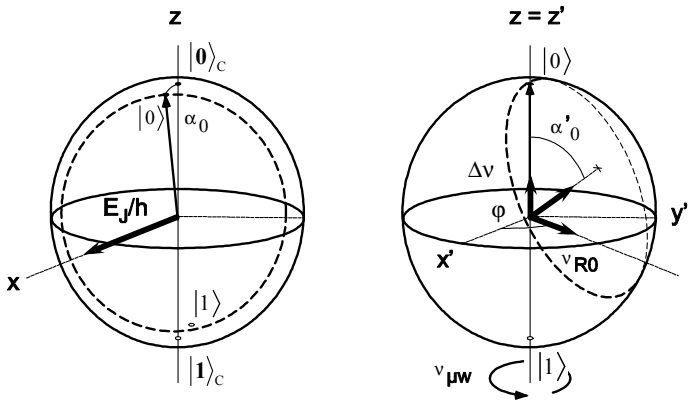

Fig. 7. Bloch sphere representations showing how the CPB state has been manipulated in two different types of experiments. The left sphere with two adjacent pure charge states at the north and south poles corresponds to a CPB with $E_J/E_C << 1$, which is driven to the charge degeneracy point with a fast dc gate pulse. The right sphere with energy eigenstates at the poles describes within the rotating wave approximation how a CPB is driven with microwave voltage pulses (see text for detailed explanation). The spin is represented by a thin arrow whereas fields are represented by bold arrows. The dotted lines show the spin trajectory, starting from the ground state.

suddenly to $N_{g0} = 1/2$ in a time so short that the evolution of the spin during this transition is negligible. Now $\vec{H} = E_J\vec{x}$ induces the Rabi precession of the spin around the x axis at the Rabi frequency

$$\nu_{Rabi} = E_J/h \; . \tag{3.4}$$

After a time t, the coherent superposition that is built has a weight $\cos^2\alpha_0 \sin^2\nu_{Rabi}t$ on $|\mathbf{1}\rangle_c$. N_g is then brought back suddenly to its initial value. The qubit precesses then around the initial $\vec{H}$ and can be measured (see section 3.2) in the $(|\mathbf{0}\rangle_c, |\mathbf{1}\rangle_c) \approx (|0\rangle, |1\rangle)$ basis. Any superposition state, i.e. any point on the Bloch sphere can thus be reached in a time shorter than $[E_J/2+E_C(1-2N_g)]/h$, by applying first a single pulse and by waiting then during a precise time. Besides, it is interesting to notice (the result will be used in section 5) that if $\Delta N_g = N_{g0} - 1/2 \neq 0$, the maximum probability to measure the qubit in state $|\mathbf{1}\rangle_c$ after a single pulse is strongly reduced as

$$\frac{1}{1 + (2E_C\Delta N_g/E_J)^2}. \tag{3.5}$$

The present driving method has been used successfully by two research groups [16, 17]. It has the great advantage of inducing fast Rabi oscillations that can

be observed even if the coherence time is rather short. On the other hand, one needs a very fast pulse generator with rise and fall times well below 100 ps. An alternative to this method is to use a harmonic perturbation.

3.1.2. Harmonic perturbation applied to the Hamiltonian

A second way to build superposed states is to apply a small resonant or almost resonant harmonic perturbation to the spin following the techniques developed in atomic physics and in Nuclear Magnetic Resonance. More precisely, a microwave pulse $\Delta N_g \cos(2\pi\nu_{\mu w}t + \varphi)$, with $\nu_{\mu w} \approx \nu_{01,}$ is added to the DC gate voltage and introduces in the Hamiltonian (2.13) a perturbation, which is written in the spin formalism as:

$$\vec{H}_{ex} = 4E_C\Delta N_g \cos(2\pi\nu_{\mu w}t + \varphi)\left[\langle 1|\,\widehat{N}\,|0\rangle\,\vec{x} + \Delta N_{10}\vec{z}\right]. \tag{3.6}$$

When $\nu_{\mu w}$ is close to ν_{01}, the effect of the longitudinal part $\vec{H}_{ex}.\vec{z}$ on the motion of $\vec{\sigma}$ can be neglected. Moreover the CPB is usually operated at the charge degeneracy point (see section 2) where $\Delta N_{10} = 0$, so that $\vec{H}_{ex}.\vec{z} = 0$. We are thus left with the transverse perturbation whose effect on $\vec{\sigma}$ is simpler to describe in a frame $R'\{\vec{x}', \vec{y}', \vec{z}'\}$ rotating at the frequency $\nu_{\mu w}$ around $\vec{z}' = \vec{z}$. Within the so-called rotating wave approximation [18], the free Hamiltonian and the perturbation correspond in R' to:

$$\vec{H} = h\Delta\nu\,\vec{z}' \text{ with } \Delta\nu = \nu_{01} - \nu_{\mu w} \tag{3.7}$$

$$\vec{H}_{ex} \simeq h\nu_{R0}\left[\vec{x}'\cos\varphi + \vec{y}'\sin\varphi\right] \text{ with } \nu_{R0} = 2E_C\Delta N_g\,\langle 1|\,\widehat{N}\,|0\rangle\,/h\,. \tag{3.8}$$

When no microwave signal is applied to the gate, $\vec{\sigma}$ precesses freely in R' around $\vec{z}'$ at the detuning frequency $\Delta\nu$, whereas during microwave pulses, it precesses around $\vec{H} + \vec{H}_{ex}$ (see right panel of Fig. 7) at the Rabi frequency

$$\nu_{Rabi} = \nu_{R0}\sqrt{1 + \left(\frac{\Delta\nu}{\nu_{R0}}\right)^2}\,,$$

which is proportional to the dimensionless microwave amplitude ΔN_g when detuning $\Delta\nu$ is chosen well below ν_{R0}. Starting from $|0\rangle$, the probability to measure $|1\rangle$ after a single pulse with effective duration t is thus $\cos^2\alpha_0'\sin^2\nu_{Rabi}t$, with $\tan(\alpha_0') = \nu_{R0}/\Delta\nu$. Note that the rise and fall time of the microwave pulses do not need to be short and that the precession axis and the Rabi frequency are tunable through the three parameters ΔN_g, $\nu_{\mu w}$, and φ. Moreover, any single qubit gate (i.e. any rotator operating on the Bloch sphere) can be implemented with a sequence of resonant pulses along $\vec{x}'$ and $\vec{y}'$ only [19], and all the tricks developed in NMR like composite pulse techniques [18] are applicable.

This microwave driving method has been successfully applied to a split box [20] with $E_J/E_C \sim 1$, and also to phase [2] and flux [3] Josephson qubits.

3.1.3. Adiabatic acceleration

Finally, we also mention here an alternative way to perform a rotation around $\vec{z}'$, using a technique transposed from the "Stark pulse technique" known in atomic physics [21]. It consists, starting from a freely evolving superposed state

$$a\,|0\rangle + b\exp\left[2\pi\nu_{01}\left(Ng_0,\delta_0\right)t\right]|1\rangle\,,$$

in applying a closed adiabatic variation of the external parameters N_g and δ away from and back to the working point (N_{g0},δ_0) in order to decrease or increase temporarily the deterministic relative dephasing speed $2\pi\nu_{01}\left(N_g,\delta\right)$ between components $|0\rangle\left(N_g,\delta\right)$ and $|1\rangle\left(N_g,\delta\right)$, without changing their weights. This method has been successfully tested with the split box mentioned above by moving adiabatically N_g away from and back to $(N_{g0}=1/2,\delta_0=0)$ along the bold line of Fig. 12.

3.2. Readout of Cooper pair box quantum states

Many different strategies [13–16,22–24,26,27] have been proposed to distinguish the $|0\rangle$ and $|1\rangle$ states of a CPB. For some of them, the readout is coupled to the box charge whereas for others, it is coupled directly or indirectly to the δ phase degree of freedom of a split box. In all cases, an important distinction is whether the readout device is designed to perform a projective measurement onto some $|0\rangle'$ and $|1\rangle'$ states close to $|0\rangle$ and $|1\rangle$, or if it designed to perform a non projective measurement involving a relaxation process of the box from $|1\rangle$ to $|0\rangle$. A second characteristic is whether the readout is designed to be switched off during the box manipulation and then switched on to measure it with a signal to noise ratio larger than 1 in a single shot, or if it is designed to measure continuously a box which is periodically prepared in the same coherent state, so that the signal becomes detectable only after many repetitions. Although almost all possibilities have been considered in theoretical proposals, we describe below only the methods that have been really implemented experimentally. A last important property that will be considered in section 4 is the back-action that the readout induces onto the qubit and that can limit its coherence time.

3.2.1. Box charge used to build a current through an additional tunnel junction

At a time when no ultrasensitive electrometer would have been fast enough to discriminate the average charges $\langle N_1\rangle$ and $\langle N_0\rangle$ of a CPB-based-qubit in a time shorter than its relaxation time, Y. Nakamura and co-workers added to a split CPB with $E_J/E_C \ll 1$ a clever readout, which demonstrated in 1999 the first

Rabi oscillations of an electrical circuit (see Fig. 8). A small and very opaque additional tunnel junction is connected to the island and biased with a voltage V such that an extra Cooper pair can enter the island and be broken into two electrons which then tunnel sequentially through the junction with rates Γ_{qp1} and Γ_{qp2} [16]. In the $|0\rangle$ state, this cyclic process gives rise to a finite current through the junction, the Josephson quasiparticle current (JQP) [28]. When the box is in its $|1\rangle$ state at $N_{g0} \sim 0.2 - 0.4$ with $\langle N_1 \rangle \sim 1$, it relaxes to its $|0\rangle$ state with $\langle N_0 \rangle \sim 0$ in a single JQP cycle with a relaxation rate Γ_{qp1}. By repeating rapidly the preparation of the $|1\rangle$ state, the JQP current can then be made larger than in the $|0\rangle$ state, the difference being used to measure the qubit state. Note that the coupling between the box and the readout being weak, the measured states are very close to $|0\rangle$ and $|1\rangle$, although the measurement is not projective and resets automatically the qubit to $|0\rangle$. This method is by design not single shot and the voltage V is applied continuously while the same preparation of the state is repeated, using the fast trapezoidal N_g pulse technique described in section 3.1.1.

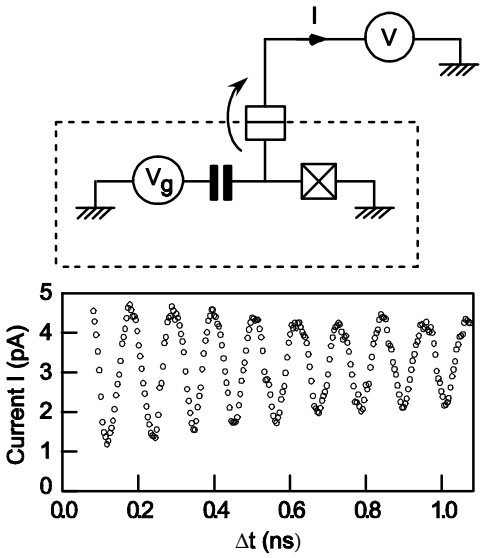

Fig. 8. First demonstration of quantum coherent control of an electrical circuit by Y. Nakamura et al. Top: simplified diagram of the setup, which includes a CPB and a readout made of a voltage biased additional opaque tunnel junction connected to the island. When fast DC pulses are applied repetitively to the CPB gate, the Josephson quasiparticle current I through the readout junction reflects the occupation probability of the CPB charge states $|\mathbf{0}\rangle_c$ and $|\mathbf{1}\rangle_c$ (see text). Bottom: Rabi oscillations of the CPB state measured by the variation of I. *Courtesy of Y. Nakamura et al., NEC, Japan.*

3.2.2. Capacitive coupling to an electrometer

The most natural way for discriminating the two CPB states is to measure the expectation value $\langle N \rangle$ of its island charge by coupling it capacitively to an electrometer. The basic single electron transistor (SET) [5] was the first electrometer used to characterize the $|0\rangle$ state of a CPB by measuring the 2e periodic Coulomb staircase [7] mentioned in section 2.4. This device has a maximum bandwidth of a few kHz and is far from being fast enough to measure the $|1\rangle$ state before it relaxes to $|0\rangle$. A faster version of the SET, the RFSET, was invented in 1998 [25] and was used by P. Delsing et al. [17] to measure a split CPB with $E_J/E_C \ll 1$, using the setup shown in Fig. 9. This RFSET includes a SET made up of an island defined by two tunnel junctions in series, biased with a voltage source. At DC voltages lower than or of the order of the Coulomb gap, the IV curve of the SET is modulated by the average charge of the CPB capacitively coupled to its island. By inserting the SET in parallel with the capacitance of a tank circuit that resonates in the radiofrequency domain and by applying a quasi-resonant RF signal to the ensemble, one measures a reflection coefficient that depends on the charge coupled to SET. The coupling between the RFSET and the CPB being weak, this readout is of the projective type. Besides, it can in principle be switched on and off with both the DC voltage and the RF input signal. Moreover, its sensitivity of the order of $10^{-5}e/\sqrt{Hz}$ is high enough and its back-action onto the qubit during the measurement is low enough that it can be operated in a single shot mode [27], provided that the qubit relaxation time is larger than or of order 1 μs. Unfortunately, at the time of writing (2003), it has proved difficult to measure a CPB in this mode. Rabi oscillations [17] were demonstrated over a few nanoseconds with the fast trapezoidal N_g pulse technique and with the RFSET operated in the continuous mode (see Fig. 9).

An important point to notice is that a CPB-based-qubit measured through its average charge $\langle N \rangle$ is usually in the regime $E_J/E_C \ll 1$, for which the signal $\Delta N_{10} \sim 1$ is maximal as soon as $N_g \neq 1/2$. Consequently, its Coulomb energy E_C is rather high and its Hamiltonian is sensitive to any external charge fluctuations. It is well known that single charge devices like the CPB have always suffered from charged two-level-fluctuators, which play the role of additional noisy gate voltage sources and can thus induce decoherence of the qubit state (see section 4). It is thus interesting to increase E_J/E_C and to find an alternative to the measurement of $\langle N \rangle$.

3.2.3. Measurement of the split box persistent current: The Quantronium

A possible alternative to measurements of $\langle N \rangle$ consists in measuring the persistent current of a split box or the magnetic field it produces. For measuring the magnetic field, the superconducting loop of the split CPB can be coupled by mutual inductance to a SQUID or to a tank circuit whose effective inductance be-

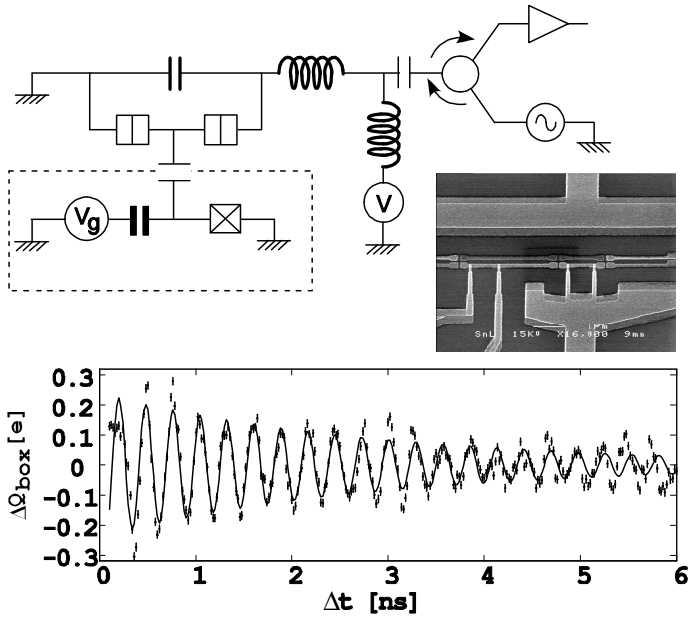

Fig. 9. Coherent control of a CPB by P. Delsing et al. Top: Simplified diagram of the setup showing that the CPB island is coupled capacitively to an RFSET, the RF reflecting power of which depends on the CPB average charge. Middle right: Scanning electron micrograph of the sample showing the SET on the left and the (split) box on the right. This sample was made by double angle shadow evaporation of aluminum through an e-beam patterned resist mask. Bottom: Rabi oscillations obtained with this readout, when applying repetitive fast DC pulses to the CPB gate. Here, ΔQ_{box} is the average charge in the box island. *Courtesy of the "Quantum Device Physics" group, Chalmers University of Technology, Göteborg, Sweden.*

comes different for the $|0\rangle$ and $|1\rangle$ CPB states, as proposed by A. Zorin et al. [14]. The latter technique is similar to that used for the RFSET and is currently under development.

We now describe the Quantronium, a setup proposed by D. Esteve [13] in order to discriminate the split box states directly through its loop persistent current. The circuit sketched in Fig. 10 consists of a split CPB with an additional current biased large Josephson junction with Josephson energy $E_{J0} \gg E_J$, inserted in the superconducting loop. During the manipulation of the qubit, the bias current I_b is kept small, so that the effective inductance of the additional junction is small and that the phase $\gamma = \arcsin(\varphi_0 I_b/E_{J0})$ across it behaves classically. The Quantronium is thus, during manipulation, a split box with $\delta = \Phi/\varphi_0 + \gamma$, the current biased junction playing only the role of an additional phase source for the split box. During the readout process, the additional junction is used to transfer adiabatically the information about the quantum state of the split box onto the phase γ, in analogy with the Stern & Gerlach experiment, where the spin state of a silver atom is entangled with its transverse position. For this transfer, a trapezoidal readout pulse $I_b(t)$ with a peak value slightly below the critical current $I_0 = E_{J0}/\varphi_0$ is applied to the circuit. Starting from $\delta = 0$, the phases $\langle\gamma\rangle$ and $\langle\delta\rangle$ grow during the current pulse and a state-dependent supercurrent develops in the loop. This current $\langle i\rangle$ adds algebraically to I_b in the large junction and modifies its switching rate Γ. By precisely adjusting the amplitude and duration of the $I_b(t)$ pulse, the large junction switches during the pulse to a finite voltage state with a large probability p_1 for state $|1\rangle$ and with a small probability p_0 for state $|0\rangle$ [13]. The switching of the large junction to the voltage state is then detected by measuring the voltage across it with an amplifier at room temperature. Although this measurement scheme is projective in a first step, it is nevertheless destructive due to the large amount of quasi particles produced when the voltage develops across the readout junction. Besides, it is designed to be single shot, its efficiency being expected to exceed $\eta = p_1 - p_0 = 95\%$ for a critical current $I_0 \sim 0.5 - 1\mu A$ and for the persistent currents plotted in Fig. 6. A Quantronium sample has been operated successfully (see Fig. 10) with the microwave N_g pulse technique, although the maximum overall efficiency of its readout was only $\eta \sim 20\%$. This sample has the longest coherence time observed so far (2004) in a Josephson qubit. The reasons for this success are analyzed in the next section devoted to decoherence of CPB-based- qubits.

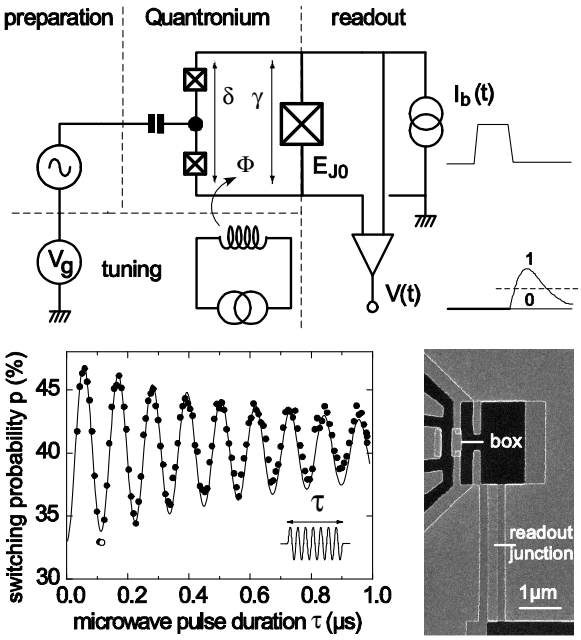

Fig. 10. Coherent control of a Quantroniun by the Quantronics group of CEA Saclay. Top: simplified diagram of the setup showing the readout Josephson junction inserted in the loop of a split box . A trapezoidal current pulse $I_b(t)$ is applied to this junction so that the latter switches out of its zero voltage state with a higher probability if the Quantronium is projected onto $|1\rangle$ than if it is projected onto $|0\rangle$. Bottom right: Scanning electron micrograph of a Quantronium made by double angle shadow evaporation of aluminum. Bottom left: Rabi oscillations obtained on a Quantronium with $E_J = 0.86 k_B K$ and $E_C = 0.68 k_B K$ when applying repetitively a resonant microwave pulse to the gate and a current pulse to the readout junction. Each experimental point is an average over 5×10^4 sequences.

4. Decoherence of Josephson charge qubits

4.1. Evaluation of decoherence: a simple approach

As with cany other quantum object, CPB-based-qubits are subject to decoherence due to their interaction with uncontrolled degrees of freedom present in their environment. From a general point of view, these interactions between the CPB and its environment entangle them in a complex way, which can be analyzed in principle by writing the total Hamiltonian of the system {CPB+environment} and by computing the evolution of the qubit reduced density matrix. Although this method has been used successfully for calculating decoherence induced by an RFSET [29] reading a CPB, it is in practice intractable in many cases. Moreover, it does not lead to analytical expressions showing directly the influence of each parameter and of each decoherence source, so that it is not always of great help for designing an experiment. Fortunately, decoherence during the free evolution of the qubit can be described in a much simpler way when the coupling between the qubit and its environment is weak. Indeed, an external parameter λ (such as N_g or δ) entering the Hamiltonian $\widehat{H} = -1/2\,\overrightarrow{\sigma}\cdot\overrightarrow{H}(\lambda)$ submitted to small quantum fluctuations from the external degrees of freedom can be treated as an operator of the environment. More precisely, each independent part X of the environment plays the role of an independent quantum noise source on the centered operator $\widehat{\lambda}_0 = \widehat{\lambda} - \langle\lambda\rangle$. To first order, the coupling Hamiltonian between this source and the CPB is written

$$\widehat{H}_X = -1/2\left(\overrightarrow{D}_\lambda\cdot\overrightarrow{\sigma}\right)\widehat{\lambda}_0^X\,, \tag{4.1}$$

where $\overrightarrow{D}_\lambda\cdot\overrightarrow{\sigma}$ is the restriction of $-2\widehat{\partial H/\partial\lambda}$ to the $\{|0\rangle\,,|1\rangle\}$ space. Then, from the noise properties of each source X, one calculates separately three relevant quantities that characterize X-induced decoherence: the first two characterize the depolarization of the fictitious spin representing the qubit. They are the excitation $\Gamma_{\uparrow,X}$ and relaxation $\Gamma_{\downarrow,X}$ rates giving the probability per unit time of X-induced $|0\rangle \rightarrow |1\rangle$ and $|1\rangle \rightarrow |0\rangle$ transitions of the qubit, respectively. The third relevant quantity is the "dephasing function" $f_X(t) = \langle\exp[i\Delta\varphi_X(t)]\rangle$ involving the X-induced random dephasing $\Delta\varphi_X(t)$ between the two components of a superposed state $a(t)\,|0\rangle + b(t)\exp[i\Delta\varphi_X(t)]\,|1\rangle$ (note that $f_X(t)$ is not necessarily exponential and characterized by a rate). The evolution of the qubit density matrix is then easily deduced from the values of $\Gamma_{\uparrow,X}$, the values of $\Gamma_{\downarrow,X}$ and the $f_X(t)$ functions. Introducing the total dephasing function $F(t) = \prod_X f_X(t)$ and the total upward and downward rates $\Gamma_\uparrow = \sum_X \Gamma_{\uparrow,X}$ and $\Gamma_\downarrow = \sum_X \Gamma_{\downarrow,X}$, the diagonal elements evolve exponentially towards their equilibrium values $1-\epsilon$ and $\epsilon = \Gamma_\uparrow/\Gamma_1$ with the characteristic rate $\Gamma_1 = \Gamma_\uparrow + \Gamma_\downarrow$, whereas off-diagonal

elements decay as $F_2(t) = \exp[-\Gamma_1 t/2]F(t)$. In the next sections, we calculate explicitly $\Gamma_{\uparrow,X}, \Gamma_{\downarrow,X}$ and $f_X(t)$ for the main decoherence sources X , in the case when the noise $\widehat{\lambda}_0^X$ is Gaussian and can be fully characterized by a generalized quantum spectral density function of angular frequency ω [1]:

$$S_{\lambda_0}^X(\omega) = \frac{1}{2\pi}\int_{-\infty}^{+\infty} d\tau \left\langle \widehat{\lambda}_0^X(t)\widehat{\lambda}_0^X(t+\tau)\right\rangle \exp(-\mathbf{i}\omega\tau). \tag{4.2}$$

In this expression, the prefactor is chosen so that $S_{\lambda_0}^X(\omega)$ coincides in the classical limit and at low frequency with the spectral density of the engineer. Note that $S_{\lambda_0}^X(\omega)$ is defined for positive and negative ω's, the positive and negative parts being proportional to the number of environmental modes that can absorb and emit a quantum $\hbar\omega$, respectively.

4.2. Overview of decoherence sources in a CPB

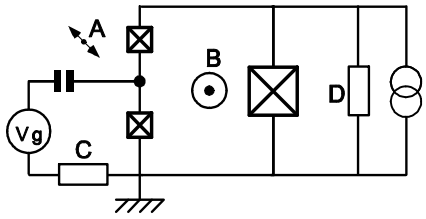

Fig. 11. Main decoherence sources in a Quantronium device. Quantum noise on N_g is generated by charged two-level-fluctuators (A) located near the CPB island and by voltage fluctuations of the series impedance (C) in the gate line. Quantum noise on δ is generated by fluctuations of the magnetic field (B) and by current fluctuations of the finite impedance (D) in parallel with the current bias source of the readout.

The uncontrolled degrees of freedom coupled to the idealized CPB of section 2 include those of the CPB substrate, those of the electrical lines of the driving and readout circuitry, and also the CPB's microscopic internal degrees of freedom which have been considered as frozen up to now. As an example, Fig. 11 shows the main decoherence sources in a Quantronium device (see section 3.2.3), which are now presented briefly.

Background charge noise First, microscopic charged two-level-fluctuators (A in Fig. 11) always present near the CPB island, either on the substrate or inside the Josephson junctions, are coupled to $\widehat{N}$ and act on the box as additional uncontrolled N_g sources. Although this background charge noise (BCN) is out of equilibrium and its generalized quantum spectral density is unknown, its classical

spectral density $\widetilde{S}_{N_g,}^{BCN}(\omega) \sim B/|\omega|$ has been measured up to the MHz region, the values found for B being of order $10^{-7} - 10^{-9}$.

Impedance of the gate line The finite series impedance Z_g in the gate line (C in Fig. 11) can be regarded as an infinite collection of harmonic oscillators [1] also coupled to $\widehat{N}$ and inducing quantum noise on N_g. The circuit as seen from the pure Josephson element of the CPB (junction capacitance not included) is equivalent [9] to an effective gate capacitance C_Σ in series with a voltage source $\kappa_g V_g$ having an internal impedance Z_{eq}. In the weak coupling limit defined by $\kappa_g = C_g/C_\Sigma \ll 1$ and for all relevant frequencies, the real part of Z_{eq} is written:

$$\mathrm{Re}[Z_{eq}] \simeq \kappa_g^2 \,\mathrm{Re}[Z_g]\,. \tag{4.3}$$

At thermal equilibrium at temperature T, Z_{eq} generates voltage fluctuations whose spectral density S_u corresponds to N_g fluctuations with spectral density $S_{N_g}^{Z_g}$:

$$S_u = \frac{\hbar\omega}{2\pi}\left[1 + \coth\left(\frac{\hbar\omega}{2k_BT}\right)\right]\mathrm{Re}[Z_{eq}], \tag{4.4}$$

$$S_{N_g}^{Z_g} = \left(\frac{C_\Sigma}{2e}\right)^2 S_u \simeq \kappa_g^2 \frac{\hbar^2\omega}{E_C^2}\left[1 + \coth\left(\frac{\hbar\omega}{2k_BT}\right)\right]\frac{\mathrm{Re}[Z_g]}{R_k}\,, \tag{4.5}$$

where $R_k = h/e^2 \simeq 26k\Omega$.

Magnetic flux noise Fluctuations of the magnetic field threading the loop of a split CPB (B in Fig. 11), either due to the motion of vortices in the vicinity of the loop or more macroscopically due to the current noise in the wires producing the field, generate directly δ noise. When the noise source is a circuit inductively coupled to the loop, its spectral density can be easily derived following the same method as we follow below for calculating the back-action of a Quantronium readout.

Readout back-action For a CPB measured by an RFSET (see section 3.2.2), the stochastic tunneling of electrons into and out of the SET island generates quantum noise on N_g. The reader can refer to [27, 29] for a characterization of this noise. For the Quantronium, the back-action of the readout circuit is the quantum noise on δ induced by the finite admittance Y_R in parallel with its current source (D in Fig. 11). More precisely, when a bias current $I_b < I_0$ is applied to the Quantronium, small oscillations of the phase δ are centered on $\delta_0 \simeq \arcsin(I_b/I_0)$ and the readout junction behaves as an inductance $L_{J0} \simeq \varphi_0/[I_0\cos\delta_0]$ much smaller than the inductance L_J of the box junction . Y_R and

L_{J0} form together an effective admittance $Y_{R,eq} = Y_R // L_{J0}$ that generates current fluctuations characterized by the spectral density

$$S_I = \frac{\hbar\omega}{2\pi}\left[1 + \coth\left(\frac{\hbar\omega}{2k_BT}\right)\right] \mathrm{Re}[Y_R\,]. \tag{4.6}$$

$|Y_R\,|$ being much smaller than the effective inductance of the series combination of the two CPB Josephson junctions, this current I goes through $Y_{R,eq}$ and is converted into noise on voltage $v = \varphi_0 d\delta/dt = I/Y_{R,eq}$, or equivalently into a δ noise with spectral density

$$S_\delta^{Y_R} \simeq \left(\frac{1}{\varphi_0\omega}\right)^2 \frac{S_I}{\left|Y_R + \frac{1}{iL_{J0}\omega}\right|^2}\,. \tag{4.7}$$

Internal decoherence sources Finally, as examples of internal decoherence sources, one can think of out-of-equilibrium quasiparticles tunneling across the Josephson junctions or of an atom in the CPB Josephson junction jumping back and forth between two atomic sites so that a tunneling channel of the junction is open and closed randomly, such that it induces noise on E_J. Note that part of the decoherence of Josephson phase qubits has been attributed to this latter phenomenon [2].

4.3. Depolarization of a Cooper pair box

Relaxation and excitation proceed by exchange of an energy quantum $\hbar\Omega_{01}$ between the qubit and an oscillating field of the environment with pulsation $\omega = \Omega_{01} = 2\pi\nu_{01}$. Applying the Fermi golden rule to such processes gives:

$$\Gamma_{\downarrow,X} = \frac{\pi}{2}\left(\frac{D_{\lambda,\perp}}{\hbar}\right)^2 S_{\lambda_0,X}(\Omega_{01}), \tag{4.8}$$

$$\Gamma_{\uparrow,X} = \frac{\pi}{2}\left(\frac{D_{\lambda,\perp}}{\hbar}\right)^2 S_{\lambda_0,X}(-\,\Omega_{01})\,, \tag{4.9}$$

where the transverse part of $\overrightarrow{D}_\lambda$, $D_{\lambda,\perp} = 2|\,\langle 1|\,\widehat{\partial H/\partial\lambda}\,|0\rangle\,|$, is equal to $4E_C|\,\langle 0|\,\widehat{\mathbf{N}}\,|1\rangle\,|$ for all N_g noise sources and equal to $2\varphi_0|\,\langle 0|\,\widehat{\mathbf{I}}\,|1\rangle\,|$ for all δ noise sources, according to (2.13) and (2.15), respectively. Going further requires then specifying the origin of the noise. For the background charge noise, the spectral density is unfortunately unknown in the GHz range that corresponds to Ω_{01} so that no serious prediction of $\Gamma_{\downarrow,X}$ and $\Gamma_{\uparrow,X}$ can be made. For the gate line impedance

$Z_g(\omega)$ at a temperature $T \ll \hbar\Omega_{01}/k_B$, $S_{N_g,Z_g}(-\Omega_{01})$ and $S_{N_g,Z_g}(\Omega_{01})$ obey detailed balance and

$$\frac{\Gamma_{\uparrow,Z_g}}{\Gamma_{\downarrow,Z_g}} = \exp(-\frac{\hbar\Omega_{01}}{k_B T}) \ll 1 .$$

Then, after substituting $D_{\lambda,\perp}$ and (4.5) at zero temperature in (4.8), one gets the relaxation rate

$$\Gamma_{\downarrow,Z_g} = 16\pi\kappa_g^2 \left|\langle 0|\,\widehat{\mathbf{N}}\,|1\rangle\right|^2 \frac{\mathrm{Re}[Z_g(\Omega_{01})]}{R_k}\Omega_{01} , \tag{4.10}$$

which takes the simpler form $\Gamma_{\downarrow,Z_g} = 4\pi\kappa_g^2\Omega_{01}\sin^2\alpha\,\mathrm{Re}[Z_g(\Omega_{01})]/R_k$ in the limit $E_J/E_C \ll 1$. In conclusion, a $\mathrm{Re}[Z_g(20\mathrm{GHz})]$ as large as 10Ω coupled with $\kappa_g \sim 1-2\%$ would induce relaxation of a CPB having a $1k_BK$ transition energy with a rate of only $0.1\sin^2\alpha$ MHz.

We evaluate now the relaxation induced by a resistance $R = 1/Y_R$ in parallel with the Quantronium readout junction. Substituting $D_{\lambda,\perp}$ and (4.7) at zero temperature in (4.8), one obtains after simple algebraic transformations:

$$\Gamma_{\downarrow,R} = \frac{2\left|\langle 0|\,\widehat{\mathbf{I}}\,|1\rangle\right|^2}{\hbar\Omega_{01}} \frac{R}{\left|1+\frac{R}{iL_{J0}\Omega_{01}}\right|^2} , \tag{4.11}$$

which simplifies to $\Gamma_{\downarrow,R} = 2|\,\langle 0|\,\widehat{\mathbf{I}}\,|1\rangle\,|^2 R/(\hbar\Omega_{01})$ for $R \ll L_{J0}\Omega_{01}$. At $N_g = 1/2$, $\langle 0|\,\widehat{\mathbf{I}}\,|1\rangle$ increases linearly with the asymmetry d between the box junctions. $\Gamma_{\downarrow,R}$ varies as d^2 and a Quantronium with a $1k_BK$ transition energy and an asymmetry $d = 5\%$ would relax with a rate of order 1 MHz under the influence of a readout resistance $R = 2\Omega$ at 20 GHz. Obtaining balanced junctions during the fabrication of a Quantronium is thus an important point.

4.4. Random dephasing of a Cooper pair box

In a semi-classical approach, the random phase $\Delta\varphi_X(t)$ between the two components of a superposed state is obtained by integration of the longitudinal fluctuations of $\widehat{H}_X$:

$$\Delta\varphi_X(t) = \frac{D_{\lambda,z}}{\hbar}\int_0^t \lambda_0^X(t')dt' , \tag{4.12}$$

where the longitudinal part of $\overrightarrow{D}_\lambda$, $D_{\lambda,z} = \langle 0|\,\widehat{\partial H/\partial\lambda}\,|0\rangle - \langle 1|\,\widehat{\partial H/\partial\lambda}\,|1\rangle \approx h\partial\nu_{01}/\partial\lambda$, is equal to $-2E_C\,\Delta N_{10}$ for all N_g noise sources and equal to $-\varphi_0\Delta i_{10}$

for all δ noises sources, according to sections 2.4 and 2.6. An important point to notice is that the coefficients of sensitivity to charge and phase noise, $D_{Ng,z}$ and $D_{\delta,z}$, vanish when ΔN_{10} and Δi_{10} are equal to zero, i.e. at $N_g = 0$ and $\delta = 0$, where the transition frequency is stationary. Then, $\lambda_0^X(t)$ being a Gaussian noise in most cases, the ensemble average $f_X(t) = \langle \exp[i\Delta\varphi_X(t)] \rangle$ is written

$$f_X(t) = \exp[-\left\langle \Delta\varphi_X^2(t) \right\rangle /2] \tag{4.13}$$

and depends only on the variance of the random phase, which can be calculated from the classical spectral density $\widetilde{S}_{\lambda_0}^X(\omega)$ of λ_0^X:

$$\left\langle \Delta\varphi_X^2(t) \right\rangle = \left(\frac{D_{\lambda,z}}{\hbar} t \right)^2 \int_{-\infty}^{+\infty} d\omega \; \widetilde{S}_{\lambda_0}^X(\omega) \mathrm{sinc}^2(\frac{\omega t}{2}) \; , \tag{4.14}$$

with $\mathrm{sinc}(x) = \sin(x)/x$. A full quantum calculation [9] of $f_X(t)$, based on a thermal average over a bath of harmonic oscillators linearly coupled to $\widehat{\lambda}$, gives the same result:

$$f_X(t) = \exp\left[-\frac{t^2}{2} \left(\frac{D_{\lambda,z}}{\hbar} \right)^2 \int_{-\infty}^{+\infty} d\omega \; S_{\lambda_0}^X(\omega) \mathrm{sinc}^2(\frac{\omega t}{2}) \right] \; , \tag{4.15}$$

but with $\widetilde{S}_{\lambda_0}^X$ being replaced by its quantum analogue. Applied to the background charge noise, (4.15) becomes

$$f_{BCN}(t) = \exp\left[-B \left(\frac{2E_C \; \Delta N_{10}}{\hbar} \right)^2 t^2 \ln \frac{\tau}{t} \right] \; , \tag{4.16}$$

where τ is the time taken experimentally to define the average transition frequency, this time introducing a low frequency cutoff $1/\tau$ in the integral of (4.15). The function $f_{BCN}(t)$ decays almost as a Gaussian with an effective characteristic time $T_2^{*BCN} = [2\sqrt{B \ln(\tau/t)} E_C \; \Delta N_{10}/\hbar]^{-1}$ that decreases almost as $1/(N_g - 1/2)$ close to the charge degeneracy (see the ΔN_{10} variations of Fig. 2). Assuming $B \sim 10^{-8}$ and $\tau \sim 10^2 s$, one gets $T_2^{*BCN} \sim 50ns$ for a CPB with $E_J \sim E_C \sim 1 k_B K$ operated at $N_g = 0.55$.

In contrast to $\widetilde{S}_{N_g,}^{BCN}(\omega)$, spectral densities $S_{\lambda_0}^X(\omega)$ of other noise sources are often rather flat below a cut-off frequency ω_c, so that for $t > 1/\omega_c$, $S_{\lambda_0}^X(\omega) \approx S_{\lambda_0}^X(0)$ in the ω range where the sinc square term gives its main contribution to the integral in (4.15). Consequently, $f_X(t) \approx \exp[-\Gamma_\varphi^X t]$ with a decay rate

$$\Gamma_\varphi^X \approx \pi \left(\frac{D_{\lambda,z}}{\hbar} \right)^2 S_{\lambda_0}^X(\omega \approx 0) \; . \tag{4.17}$$

At 50 mK, spectral densities (4.5) and (4.7) vary only by a factor two below 200 MHz so that (4.17) holds for $t > 5ns$. Substituting the correct $D_{\lambda,\perp}$ and (4.5) [resp. (4.7)] at zero frequency in (4.17), one finds the contribution to random dephasing of the gate line circuit (resp. of the Quantronium readout):

$$\Gamma_{\varphi}^{Z_g} \approx 8\pi\kappa_g^2 \Delta N_{10}^2(N_{g0}) \frac{k_B T}{\hbar} \frac{R}{R_k} \ , \tag{4.18}$$

$$\Gamma_{\varphi}^{R} \approx \frac{1}{8\pi} \left(\frac{\Delta i_{10}(\delta_0)}{I_0 \cos\delta_0} \right)^2 \frac{k_B T}{\hbar} \frac{R_k}{R}, \tag{4.19}$$

where R is the resistance of the gate voltage source (4.18) and the resistance in parallel with the Quantronium readout junction in (4.19), in the 0.1-100 MHz frequency range. Taking the same CPB parameters as in the previous section and assuming an electronic temperature of 50 mK, one gets $\Gamma_{\varphi}^{Z_g} < 25$kHz for $R = 10\Omega$, showing that the gate line is not an important dephasing channel. Assuming then typical values $I_0 \sim 500nA$ and $R = 100\Omega$ for a Quantronium readout circuit, one obtains $\Gamma_{\varphi}^{R} \sim 2\delta_0^2(rad)/\cos^2\delta_0$MHz. Therefore, Γ_{φ}^{R} is negligible close to $\delta_0 = 0$ and increases very rapidly up to about 100 MHz at the top of the readout current pulse, where δ approaches $\pi/2$.

4.5. Design rules and optimal working points

We now focus on the requirements that an experimental setup has to fulfill in order to demonstrate an operational CPB-based-qubit. First, the CPB has to be reset in its reference stable state $|0\rangle$ with a small probability of error $e \geq \epsilon = \Gamma_{\uparrow}/\Gamma_1$. This takes a reset time $t_r \sim e/\Gamma_1$ that defines the maximum repetition rate in an experiment. Secondly, during the manipulation of the state, the characteristic decay time T_2^* of $F_2(t)$ must be as long as possible in order to perform as many coherent single qubit or two qubit gate operations as possible. Consequently, $T_1 = 1/\Gamma_1$ and the characteristic decay time T_{φ}^* of the F function have to be maximized. For that purpose, a first action is of course to minimize all the noise spectral densities of section 4.2. A complementary approach is to choose a working point where the sensitivity to noise is minimal. For a split box, according to sections 4.3 and 4.4, T_1 and the T_{φ}^*'s can be maximized by choosing a manipulation point such that $\langle 1| I |0\rangle \simeq 0$ and such that the transition frequency is stationary with respect to both N_g and δ fluctuations. Figure 12 shows that the point $(N_g = 1/2, \delta = 0)$ is such an "optimal manipulation point". But since both charge signal ΔN_{10} and current signal Δi_{10} vanish at this point, one has to apply a shift to N_g or δ at the end of the manipulation to measure the qubit state through the charge or phase port. Then, the elementary measuring time t_{m0}, defined as the time during which the readout interacts with the qubit after the

preparation of a particular quantum state, is constrained in a way that depends on the readout strategy. When the readout absorbs the transition energy of the qubit as described in section 3.2.1, the readout port must be the main relaxation channel in order to avoid errors. Therefore, the values of $\Gamma_{\downarrow,X}$ and t_{m0} must obey $1/\Gamma_1 \simeq 1/\Gamma_\downarrow \simeq 1/\Gamma_{\downarrow,readout} \leq t_{m0}$. In all other cases, a readout error probability smaller than e_r requires $e_r T_1 > t_{m0}$. Consequently, we wish to maximize T_1 during readout by choosing a measurement point where $\langle 1| I |0\rangle \simeq 0$ as well. Moreover, t_{m0} has to be longer than T_φ^* since the qubit density matrix has to become diagonal before a projective measurement is completed. Since dephasing is required only during measurement, it is thus a good design rule to implement a switchable readout device such that T_φ^* decreases by several orders of magnitude when the readout is switched on, whereas T_1 remains long. Moving away from an "optimal manipulation point" along a "slow relaxation line" is just such a switch. Finally, it is convenient to have a single shot readout, able to distinguish the two qubit states with a small error rate e_r within the time t_{m0}. Otherwise, repeating several times the preparation and the measurement of the same quantum state is required to reach the same target error rate. The Quantronium has been designed to fulfill all the requirements mentioned here and has demonstrated experimentally good quantum coherence properties, which are presented in the next section.

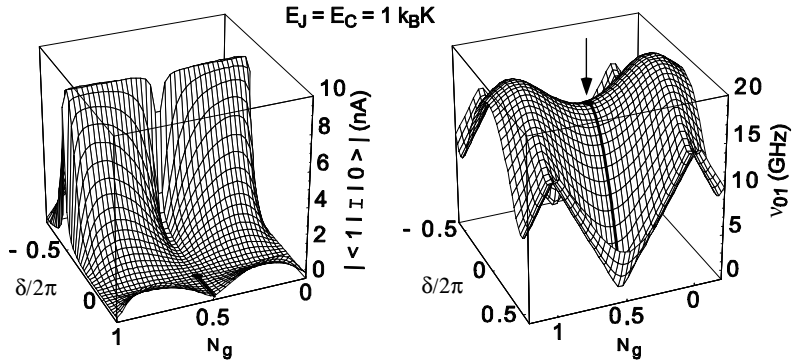

Fig. 12. Sensitivity to decoherence of a Quantronium with $E_J = E_C = 1 k_B K$ and $d = 2\%$, as a function of its reduced external parameters N_g and $\delta/2\pi$. Left box: Loop current matrix element between states $|0\rangle$ and $|1\rangle$. This matrix element and consequently the relaxation rate of the qubit are minimal along the lines $\delta = 0$ and $N_g = 1/2$. Right box: Transition frequency of the Quantronium. The arrow indicates the stationary point ($N_g = 1/2$, $\delta = 0$) where pure dephasing vanishes to first order. Consequently, this is the optimal point for coherent manipulation of the Quantronium. For reading out the state, the working point is adiabatically moved along the bold solid line, where relaxation of the qubit induced by quantum noise on δ is minimal.

4.6. Experimental characterization of decoherence

The results presented below have been obtained with a Quantronium sample similar to that shown in Fig. 10, with $E_J = 0.86 k_B K$, $E_C = 0.68 k_B K$, and an asymmetry d between the CPB junctions not precisely known, but lower than 5%. We first measured the relaxation time at the optimal working point by switching on the readout at some variable time t_d after applying a microwave π pulse that prepares the qubit in state $|1\rangle$ (see Fig.13). A rough estimation of the readout resistance of the setup giving $R(20GHz) = 1\Omega - 5\Omega$, the experimental $T_1 = 1.8\mu s$ could be explained by an asymmetry coefficient $d \sim 5\% - 2\%$.

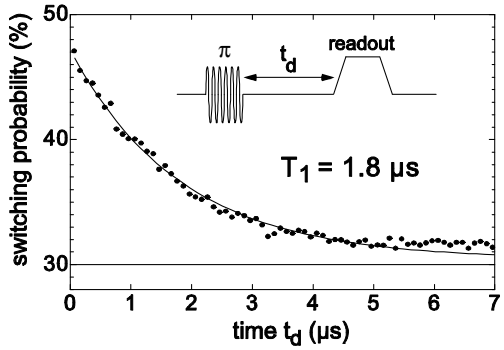

Fig. 13. Decay of the switching probability of the Quantronium's readout junction as a function of the delay between a microwave π pulse and the readout current pulse. The solid line is a fit of the data (dots) by an exponential shifted by the signal measured when no microwave is applied (horizontal bottom line).

Then, spectroscopic measurements (see Fig. 14) of ν_{01}were performed by applying to the gate a weak continuous microwave irradiation suppressed just before the readout current pulse. The variations of the switching probability as a function of the microwave frequency, display a resonance peak whose position ν_{01} as a function of N_g and δ leads to a precise determination of E_J and E_C. The resonance line shape being the Fourier transform of $F_2(t)$, the full line width at half-maximum $\Delta\nu_{01}$ leads to an effective coherence time $T_2^* = c/\Delta\nu_{01}$with $c \sim 1/\pi$ depending on the exact line shape. As expected, $\Delta\nu_{01}$ was found to be minimal at the optimal point ($N_g = 1/2, \delta = 0$), where $\Delta\nu_{01} = 0.8$ MHz. Consequently, $2T_1 \gg T_2^* \simeq 0.4\mu s \simeq T_\varphi^*$ and decoherence is dominated by random dephasing. When departing from the optimal point, the line broadens very rapidly. For $N_g \neq 1/2$, it also becomes structured and not reproducible (see top right panel of Fig. 14) due to individual charged two-level-fluctuators. Nevertheless, the general trend (see bottom panel of Fig. 14) is

that $\Delta\nu_{01}$ varies more or less linearly with $N_g - 1/2$ and δ, the proportionality coefficients $\partial\Delta\nu_{01}/\ \partial(\delta/2\pi)$ and $\partial\Delta\nu_{01}/\ \partial N_g$ being of order 0.3GHz. Noticing that ν_{01} varies quadratically in the vicinity of the optimal point so that $D_{\lambda,z} \approx h\partial\nu_{01}/\partial\lambda \propto \lambda \propto \Delta\nu_{01}$, one deduces from section 4.4, that both charge and phase noises are peaked at low frequencies and that the random dephasing functions should decay as Gaussians. This effect is well understood for the charge noise, which is dominated by the 1/f contribution of microscopic origin. Using the actual parameters of the sample in (4.16), the experimental $\partial\Delta\nu_{01}/\ \partial N_g$ leads to an amplitude $B \simeq 10^{-7}$ for the BCN, a value in agreement with previous measurements on similar Josephson devices. By contrast, the origin of the low frequency phase noise is not understood. An important point to mention here is that the experimental value of T_2^* at the optimal working point corresponds to that estimated by taking into account the second order contribution of the charge and phase noises.

The direct measurement of the coherence time T_2^* during free evolution was obtained by performing a Ramsey-fringe-like experiment (see also [21]). One applies to the gate two slightly off-resonance $\pi/2$ microwave pulses separated by a delay Δt during which the spin representing the qubit state precesses freely at frequency $\Delta\nu$ in the equatorial plane of the Bloch sphere. Whereas the first pulse simply sends the spin onto the equator, the second one converts the phase accumulated during Δt into a longitudinal component of the spin. The probability to measure $|1\rangle$ at the end of the sequence oscillates as $\cos^2(\pi\Delta\nu\Delta t)$ with an amplitude that decays as $F_2(t)$. Figure 15 shows the result of such an experiment performed at the optimal manipulation point. Although the low signal to noise ratio and the long term drift due to 1/f noise prevents determination of wether the decay of the oscillations is more Gaussian than exponential, a fit of the data leads to $T_2^* \simeq 0.5\mu s$, a value that corresponds to that previously deduced from the resonance line width. Given the transition period $1/\nu_{01} \sim 60$ps, the coherence time T_2^* corresponds to about 8000 free precession turns around the z axis. Assuming that a bit flip can be performed with a microwave pulse of only 30 oscillations, i.e. in a time $\sim$ 2ns, T_2^* corresponds also to the time required for about 250 bit flips.

The coherence can also be maintained artificially during a time longer than T_2^* using NMR-like echo sequences [18]. An intermediate π pulse is inserted in a Ramsey sequence, a time $\Delta t_1 < \Delta t$ after the first $\pi/2$ pulse (see Fig. 16). Assuming for instance that all rotations are performed around the y' axis of the Bloch sphere, the effect of this π pulse is to change rapidly the phase of the spin from $\varphi = 2\pi\Delta\nu\Delta t_1$ to $\varphi = \pi - 2\pi\Delta\nu\Delta t_1$. Then, the phase grows again by an amount $2\pi\Delta\nu(\Delta t - \Delta t_1)$ before the last $\pi/2$ pulse. The probability to measure $|1\rangle$ at the end of the sequence is $\sin^2[\pi\Delta\nu(\Delta t - 2\Delta t_1)]$. When $\Delta t_1 = \Delta t/2$, this probability is thus less sensitive to $\Delta\nu$ fluctuations than the Ramsey function

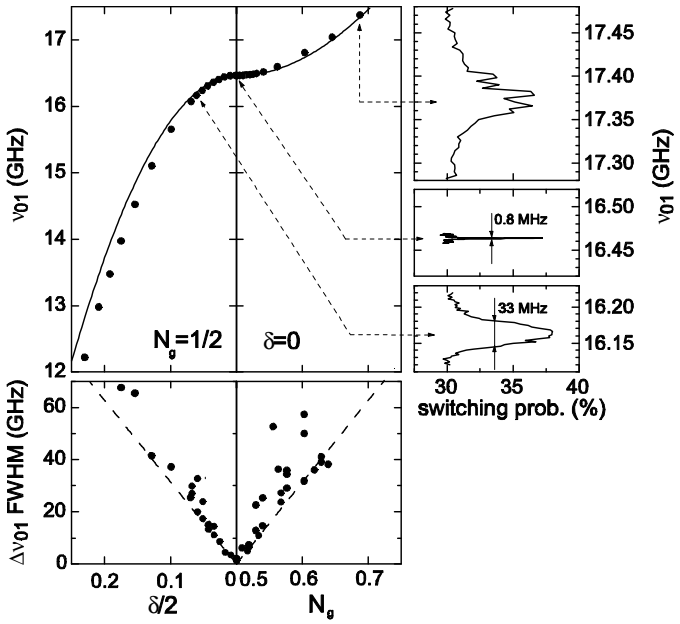

Fig. 14. Spectroscopy of a Quantronium. Top left panel: transition frequency as a function of δ at $N_g = 1/2$ and as a function of N_g at $\delta = 0$. The solid line is a fit that gives E_J and E_C. Right panels: resonance lines recorded with a small microwave power at three different working points (same scale for all lines). Bottom left panel: Full width at half-maximum $\Delta\nu_{01}$ of the resonance lines. Due to a slow and large charged two-level-fluctuator (TLF), data points can vary by a factor 2. The dotted lines indicate that $\Delta\nu_{01}$varies linearly with the external parameters when this TLF is stable.

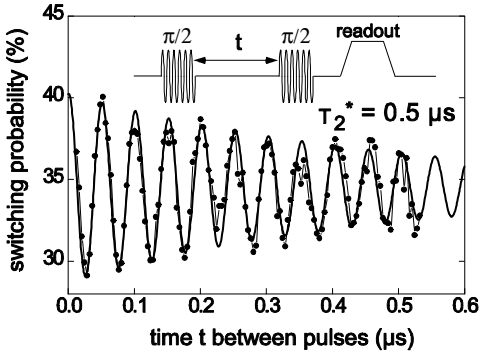

Fig. 15. Ramsey fringe experiment on a Quantronium: When two $\pi/2$ microwave pulses detuned with $\Delta\nu = 20.6$ MHz and separated by Δt are applied to the gate, the switching probability of the readout junction oscillates as a function of Δt with frequency $\Delta\nu$. Each experimental point (dot) is an average over 50000 sequences. The solid line is a fit by an exponentially decaying cosine, the decay time constant of which corresponds to the coherence time T_2^*.

$\cos^2(\pi\Delta\nu\Delta t)$. In other words, a π pulse in the middle of an echo sequence makes the spin go a longer (resp. shorter) path along the equator when the precession speed is faster (resp. slower), so that the ending point is the same from sequence to sequence, provided that $\Delta\nu$ is constant within a sequence. Figure 16 compares a Ramsey sequence and an echo sequence with variable Δt_1 performed at $N_g = 0.52$ and $\delta = 0$, where T_2^* is reduced to 30ns. For $\Delta t = 2\Delta t_1 \sim 20T_2^*$, the amplitude of the echo is still 20% of the maximum amplitude whereas the Ramsey signal is of course zero. This result confirms that decoherence is essentially due to charge noise at frequencies lower than $1/\Delta t \sim 1$ MHz. Although mapping the amplitude of the echo as a function of Δt for different working points can give much information on the shape of noise spectral densities, no complete study could be made on the sample presented here.

5. Two-qubit-gates with capacitively coupled Cooper pair boxes

Being able to implement any quantum algorithms requires adding to all possible single qubit operations a two-qubit gate such that the ensemble forms a so-called universal set of gates [30]. Many coupling schemes of two (or more) CPBs have been proposed to realize such 2-qubit gates. The nature of the coupling can be either capacitive or inductive. In the first case, two CPB islands are coupled by a capacitor, whereas in the second case, the loops of two split CPBs are coupled

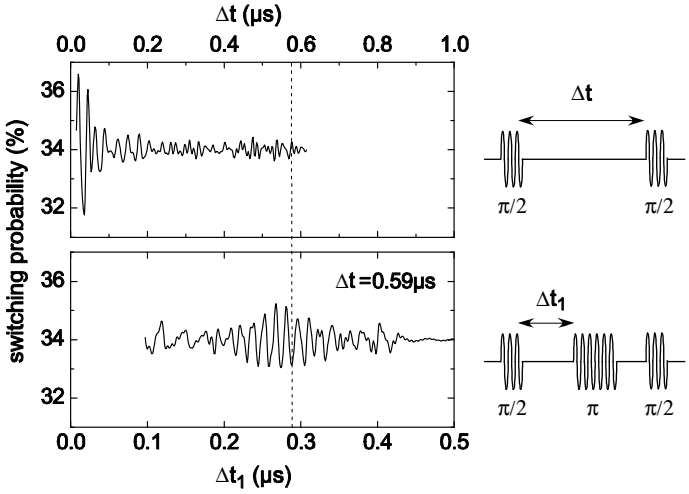

Fig. 16. Comparison between a Ramsey and an echo sequence (top right and bottom right pictograms, respectively) with a Quantronium circuit operated at the working point ($N_g = 0.52, \delta = 0$) with a detuning $\Delta\nu = 41$MHz. Top panel: Ramsey fringes of the Quantronium's switching probability indicating a coherence time of only 30 ns. Bottom panel: Echo signal taken at fixed $\Delta t = 0.59\mu s$ as a function of Δt_1. Very close to $\Delta t_1 = \Delta t/2$, the amplitude of the echo is maximum and equal to about 20% of the signal at $\Delta t = 0$. The dashed vertical line indicates Δt_1 and points out that the Ramsey signal has completely disappeared for the same Δt.

by a mutual inductance or galvanically by an inductor or an additional Josephson junction. Although ideally the coupling should be switchable and tunable, using a constant coupling is of course simpler. In this paper, we restrict ourselves to the constant capacitive coupling between two CPBs, which is the only scheme that has been implemented at the time of writing.

The Hamiltonian of two CPBs indexed 1 and 2, the islands of which are coupled by a capacitor C_C, is the sum of two terms (2.3) with Josephson energies including eventually a phase term if the box is split and with Cooper pair Coulomb energies involving now $C_\Sigma \approx C_g + C_J + C_C$, and of a coupling term

$$E_{CC}(\widehat{\mathbf{N}}_1 - N_{g1})(\widehat{\mathbf{N}}_2 - N_{g2}) \text{ with } E_{CC} \approx E_{C1}E_{C2}\frac{C_C}{(2e)^2} \ . \tag{5.1}$$

Within the spin formalism and when $E_J/E_C \ll 1$, Hamiltonian (5.1) is rewritten in the pure charge state basis $(|\mathbf{0}\rangle_{c1}, |\mathbf{1}\rangle_{c1}) \otimes (|\mathbf{0}\rangle_{c2}, |\mathbf{1}\rangle_{c2})$:

$$\begin{aligned}\widehat{H}(N_{g1}, N_{g2}) = -\frac{1}{2}\Bigg) \, E_{J1}\widehat{\sigma}_{X1} + \left[(1-2N_{g1})E'_{C1} + (1-2N_{g2})\frac{E_{CC}}{2}\right]\widehat{\sigma}_{Z1}\Bigg\} \\ - \frac{1}{2}\left\{E_{J2}\widehat{\sigma}_{X2} + \left[(1-2N_{g2})E'_{C2} + (1-2N_{g1})\frac{E_{CC}}{2}\right]\widehat{\sigma}_{Z2}\right\} \\ + \frac{E_{CC}}{4}\widehat{\sigma}_{Z1}\widehat{\sigma}_{Z2} \ ,\end{aligned} \tag{5.2}$$

where constant terms that depend only on N_{g1} and N_{g2} have been dropped. The coherent evolution induced by this Hamiltonian has been experimentally demonstrated [31] with two strongly coupled ($E_{CC} \sim E_{J1,2}$) CPBs, using fast DC gate pulses (see section 3.1.1) to the charge co-degeneracy point $N_{g1} = N_{g2} = 1/2$, and using the readout technique described in section 3.2.1. A conditional operation close to the Controlled-NOT gate has also been demonstrated [32] with the same system. The main idea behind this experiment is to regard the $\widehat{\sigma}_{Z1}\widehat{\sigma}_{Z2}$ coupling as shifting the CPB2 charge degeneracy point by a quantity that depends on the state of CPB1. Indeed, this degeneracy point is defined by $(1-2N_{g2})E'_{C2} + (1-2N_{g1} \mp 1/2)E_{CC}/2 = 0$. A gate 2 pulse bringing CPB2 to the charge degeneracy when CPB1 is in state $|\mathbf{0}\rangle_{c1}$, brings it $\Delta N_{g2} = 1/2 - E_{CC}/4E'_{C2}$ away from the degeneracy when CPB1 is in state $|\mathbf{1}\rangle_{c1}$. According to section 3.1.1, the maximum probability of $|\mathbf{1}\rangle_{c2}$ after the pulse drops rapidly with ΔN_{g2} as $1/\{1 + [2E_C\Delta N_{g2}/E_J]^2\}$, so that bit 2 can be flipped when bit 1 is in state $|\mathbf{0}\rangle_{c1}$, whereas it is almost unchanged when bit 1 is in state $|\mathbf{1}\rangle_{c1}$. Figure 17 shows the experimental results obtained by the NEC group with such a C-NOT.

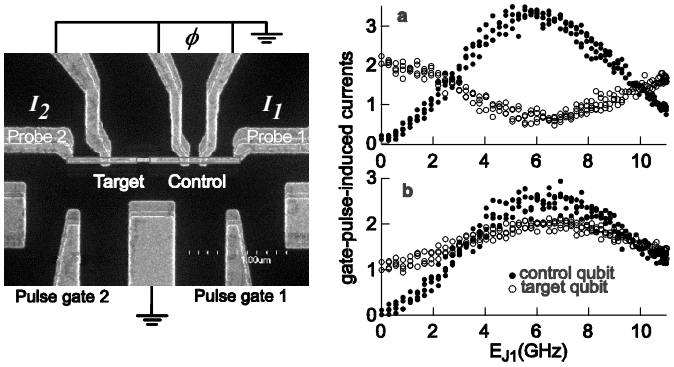

Fig. 17. Demonstration of a C-NOT-type quantum gate with two capacitively coupled CPBs by T. Yamamoto and co-workers. Left: Scanning electron micrography of the device. The qubits are manipulated using the fast dc pulse technique. Here, the target qubit is prepared in the pure charge state $|\mathbf{0}\rangle_c$ (a) or $|\mathbf{1}\rangle_c$ (b) whereas the control qubit is prepared with a dc pulse of constant width in a superposition state that depends on the Josephson energy E_{J1} of qubit 1. Finally, a gate 2 pulse performs the CNOT as explained in the text. Right panels: Anticorrelation (a) and correlation (b) between the two probe currents as a function of E_{J1}. *Courtesy of T. Yamamoto et al., NEC, Japan.*

Another type of gate can be developed by working in the uncoupled energy eigenbasis $(|0\rangle_1, |1\rangle_1)\otimes(|0\rangle_2, |1\rangle_2)$ at fixed $N_{g1} = N_{g2} = 1/2$, where $\langle 0|\,\widehat{\mathbf{N}}\,|0\rangle = \langle 1|\,\widehat{\mathbf{N}}\,|1\rangle = 1/2$. The Hamitonian (5.1) is now rewritten as

$$\widehat{H}(N_{g1}, N_{g2}) = -\frac{1}{2}h\nu_1\widehat{\sigma}_{Z1} - \frac{1}{2}h\nu_2\widehat{\sigma}_{Z2} + K\widehat{\sigma}_{X1}\widehat{\sigma}_{X2}\,, \tag{5.3}$$

with $K = E_{CC}\left|{}_1\langle 1|\,\widehat{\mathbf{N}}_1\,|0\rangle_1\right|\left|{}_2\langle 1|\,\widehat{\mathbf{N}}_2\,|0\rangle_2\right|$, the corresponding matrix being

$$\widehat{H} = \begin{pmatrix} \begin{bmatrix} -h\overline{\nu} & K \\ K & h\overline{\nu} \end{bmatrix} & [0] \\ [0] & \begin{bmatrix} -\frac{h\Delta\nu}{2} & K \\ K & \frac{h\Delta\nu}{2} \end{bmatrix} \end{pmatrix}_{(|00\rangle,|11\rangle,|01\rangle,|10\rangle)}, \tag{5.4}$$

with $\overline{\nu} = (\nu_1 + \nu_2)/2$ and $\Delta\nu = \nu_1 - \nu_2$. In the weak coupling limit defined by $C_C \ll C_{\Sigma 1,2}$, the coupling strength $K/h\overline{\nu}$ between $|00\rangle$ and $|11\rangle$ is always weak, whereas coupling strength $2K/h\Delta\nu$ between $|01\rangle$ and $|10\rangle$ can be varied by adjusting the difference between the two qubit transition frequencies. By equating ν_1 and ν_2, this coupling is maximized and $|01\rangle$ and $|10\rangle$ are simply swapped in a time $t_{SWAP} = \pi\hbar/2K$, whereas $|00\rangle$ and $|11\rangle$ are almost unchanged. When applying the effective coupling during $t_{SWAP}/2$, one obtains

the so-called $\sqrt{iSWAP}$ gate, which entangles $|01\rangle$ and $|10\rangle$ in a simple and efficient way and which forms a universal set of gates when complemented with 1-qubit operations. Moreover, the $\widehat{\sigma}_{X1}\widehat{\sigma}_{X2}$ nature of the coupling has the great advantage of conserving the property of a vanishing random dephasing at the optimal manipulation point. An experiment aiming at testing such an $\sqrt{iSWAP}$ gate prototype with two capacitively coupled Quantroniums is currently in preparation.

6. Conclusions

As anticipated in 1995 immediately after the first successful characterization of a Cooper pair box [7], this device has been shown to have sufficiently good quantum properties to be used for building quantum bit prototypes. In less than ten years, two different schemes for driving the quantum state of a CPB and three very different readouts were developed and tested in several laboratories [16, 17, 20, 25]. Spectroscopy and coherent free and driven quantum evolution were demonstrated over times ranging from a few nanoseconds up to about a microsecond. Other Josephson qubits were also able to reach comparable results and Josephson qubits should now be considered as a single family, the sub-families having only historical justifications. The research community involved in the development of Josephson qubits has made great progress in understanding how decoherence occurs in electrical circuits and "quantum electrical engineering" was really born. The concept of optimal manipulation and measuring points of such circuits could for instance be formulated and experimentally tested. Moreover, experimental protocols for characterizing decohering effects and decoherence sources are continuously improving. With the development of more complex manipulations of Josephson qubits, methods to limit decoherence such as NMR-like echoes and spin locking have already been or are about to be tested. Preliminary experiments on two coupled CPB-based-qubits have demonstrated in 2003 a first solid-state-two-qubit-gate prototype. Nevertheless, the route towards a real quantum processor incorporating, for instance, quantum error correcting circuits is still long. A good quantum-non-demolition single-shot-readout is still lacking, the precision of qubit manipulations is still weak compared to that achieved in quantum optics, and coherence times must be increased by one or two orders of magnitude to start implementing simple algorithms. Finally, the scalability of Josephson qubits is still to be demonstrated. To conclude, although we do not think that any serious prediction can be made about the future existence or not of a (Josephson) Quantum computer, we are convinced that developing Josephson qubits is a very valuable program of research

that paves the way towards a truly quantum electronics and toward machines in which quantum physics will manifest itself at a more ”macroscopic” scale.

ACKNOWLEDGEMENTS. A large part of the physics presented here, including the development of the CPB and of the Quantronium is the fruit of a collective work in the ”Quantronics group”, which is part of the condensed matter physics division (SPEC) of CEA-Saclay, France. We warmly thank the other permanent members of the group, P. Orfila, P. Senat, P. Joyez, H. Pothier, C. Urbina, M. Devoret and D. Esteve, and also the past and present post-docs and Ph.D. students, E. Turlot, P. Lafarge, V. Bouchiat, A. Cottet, A. Aassime, and E. Collin for their direct participation in the development of Josephson qubits. We also gratefully acknowledge the research group of J.S. Tsai, Y. Nakamura, and T. Yamamoto from the ”NEC Fundamental Research Lab” (Tsukuba, Japan) and the ”Quantum Device Physics” group headed by Per Delsing at Chalmers University of Technology (Göteborg, Sweden) for providing material included in this chapter. We also should like to thank very much all the people we have been collaborating with over the past ten years, in particular I. Chuang from IBM, J. Martinis from NIST, O. Buisson from CRTBT, the group of H. Mooij from Delft University, the group of G. Schön from Karlsruhe, and all our colleagues from the SQUBIT european projects. Finally, I thank N. Birge and P. Meeson who helped to improve this text.

References

[1] See chapter by M. Devoret in this book.

[2] See chapter by J. Martinis in this book.

[3] See chapter by H. Mooij in this book.

[4] A. Barone and G. Paternò, *Physics and applications of the Josephson effect* (Wiley, New York, 1982).

[5] *Single Charge Tunneling*, edited by H. Grabert and M. H. Devoret (Plenum Press, New York, 1992).

[6] M. Büttiker, Phys. Rev. B **36**, 3548 (1987).

[7] V. Bouchiat et al., Physica Scripta **76**, 165 (1998).

[8] P. Lafarge et al., Nature **365**, 422 (1993).

[9] A. Cottet, *Implementation of a quantum bit in a superconducting circuit*, Thesis, University Paris VI, Paris (2002).

[10] C. Cohen-Tannoudji, B. Diu and F. Laloë, *Mécanique quantique T II*, Hermann, Paris.

[11] D. V. Averin, K. K. Likharev, in *Mesoscopic Phenomena in Solids*, edited by B. L. Altshuler, P. A. Lee, and R. A. Webb (Elsevier, Amsterdam, 1991).

[12] A.B. Zorin, Phys. Rev. Lett. **76**, 4408 (1996).

[13] A. Cottet et al., Physica C **367**, 197 (2002).

[14] A. B. Zorin, Physica C **368**, 284 (2002).

[15] J. R. Friedman and D. V. Averin, Phys. Rev. Lett. **88**, 50403 (2002).

[16] Y. Nakamura, Yu. A. Pashkin and J. S. Tsai, Nature **398**, 786, (1999)

[17] T. Duty et al., cond-mat / 0305433 (2003).

[18] See chapter by J. Jones in this book.

[19] See chapter by I. Chuang in this book.

[20] D. Vion et al., Science **296**, 886 (2002).

[21] See chapter by M. Brune in this book.

[22] F. W. J. Hekking et al., in *Electronic Correlations: from Meso- to Nanophysics*, T. Martin, G. Montambaux and J. Trân Thanh Vân, eds. (EDP Sciences, 2001), p. 515.

[23] I. Siddiqi et al., cond-mat/0312553 (2003).

[24] See chapter by R. Schoelkopf in this book.

[25] R.J. Schoelkopf *et al.*, Science, 280, 1238 (1998).

[26] A. Cottet et al., Workshop on "Macroscopic Quantum Coherence and Computing", Naples, Italy (2001).

[27] A. Aassime et al., Phys. Rev. Lett., **86**, 3376 (2001).

[28] T.A. Fulton, P.L. Gammel, D.J. Bishop, L.N.Dunkleberger, and G.J. Dolan, Phys. Rev. Lett. 63,1307 (1989).

[29] Y. Makhlin, G. Schön and A. Schnirman, Rev. Mod. Phy, **73**, 357 (2001)

[30] M.A. Nielsen and I.L. Chuang, Quantum Computation and Quantum Information (Cambridge University Press, Cambridge, 2000).

[31] Yu. A. Pashkin et al., Nature **421**,823 (2003).

[32] T. Yamamoto et al., Nature **425**, 941 (2003).